2008

Millisecond Autothermal Steam Reforming of Cellulose for Synthetic Biofuels by Reactive Flash Volatilization

Paul J Dauenhauer, *University of Massachusetts - Amherst*
Lanny D Schmidt
Joshua L Colby

Millisecond autothermal steam reforming of cellulose for synthetic biofuels by reactive flash volatilization†

Joshua L. Colby, Paul J. Dauenhauer and Lanny D. Schmidt*

Received 19th March 2008, Accepted 25th April 2008
First published as an Advance Article on the web 2nd June 2008
DOI: 10.1039/b804691c

Three biomass-to-liquid process steps (volatilization of cellulose, tar-cleaning of organic products, and water-gas-shift of the gaseous effluent) have been integrated into a single autothermal catalytic reactor for the production of high quality synthesis gas at millisecond residence times (~30 ms). Particles of cellulose (~300 μm) were directly impinged upon the hot, catalytic bed of Rh–Ce/γ-Al_2O_3 catalyst on 1.3 mm α-Al_2O_3 spheres in the presence of O_2, N_2, and steam in a continuous flow fixed-bed reactor at 500–1100 °C. Complete conversion to gases was observed for all experimental parameters including N_2/O_2, S/C, the total flow rate of cellulose, and the fuel-to-oxygen ratio (C/O). The addition of steam increased the selectivity to H_2 and decreased the selectivity to CO in agreement with water-gas-shift equilibrium. Optimal conditions produced a clean gaseous effluent which exhibited ~80% selectivity to H_2 at a synthesis gas ratio of $H_2/CO = 2.3$ with no dilution from N_2 at a fuel efficiency of ~75%. Carbon-free processing was explained by relating the domain of experimental parameters to the thermodynamic prediction for the formation of solid carbon, C_S.

Introduction

Lignocellulosic biomass in the form of trees, grasses, and agricultural residues provides a realistic source for sustainable production of carbon-based fuels and chemicals.[1,2] Recent analysis by the U.S. Department of Agriculture estimates that annual production of lignocellulosic biomass could exceed one billion dry tons, providing sufficient energy to supplant a significant fraction of existing demand for fossil fuels.[3] The dominant structure in all non-food sources of biomass, lignocellulose, consists of the biopolymers cellulose, hemicellulose, and lignin in a design that provides optimal material properties to plant structures while resisting chemical degradation. These same properties also prevent the direct utilization of most conventional petroleum processing equipment thereby driving the development of new technology for handling and processing solid, carbonaceous materials.

Conversion of biopolymers to synthesis gas (H_2 + CO) and subsequent production of synthetic fuels is a major thermochemical processing route commonly called biomass-to-liquid (BTL). The entire BTL process consists of a combination of unit operations including biomass preparation, gasification, synthesis gas cleaning, synthesis gas processing, synthetic fuel production, and synthetic fuels refining. The availability of technologies and number of process variables for each process step provides an enormous number of configurations and design options which must be evaluated as an integrated system for optimal process development.[4] The overall process competes economically with existing biological processes (*e.g.* corn to ethanol) as demonstrated by a recent process design analysis of the BTL process for the production of ethanol from wood.[5]

The efficacy of the BTL process can be enhanced by either improving the performance of any single process step or by eliminating or combining process steps. A significant opportunity for process improvement exists with synthesis gas production and preparation. The cost of conversion to clean, conditioned synthesis gas for a synthetic fuels reactor can dominate process economics as this equipment can comprise 60–75% of the total process investment.[6,7] This paper demonstrates that at least three BTL process steps (gasification, tar-cleaning, and water-gas-shift) can be combined as a one-step millisecond residence time reactor for continuous operation. Each of these steps provides a necessary process function and contributes a non-negligible capital and operating cost. Conventional biomass gasifiers (updraft, downdraft, and fluidized bed) partially oxidize biomass to a gaseous syngas-rich effluent that commonly contains impurities such as tars and aromatics, unconverted oxygenated organics, nitrogen-containing species such as NH_3 or HCN, and soot.[8] Organic impurities must be selectively removed to ppm levels by one of several technologies that can be categorized into wet scrubbing, dry scrubbing, or hot gas conditioning.[9] Existing techniques applicable to the integrated reactor considered here include steam reforming and partial oxidation of tars and organics using Ni, Pt, or Rh metal catalysts. Biomass-derived synthesis gas typically exhibits a $H_2/CO \sim 1.0$, and an additional process step must also be used to adjust the ratio of H_2 to CO by the water-gas-shift reaction for synthetic fuel reactors to produce Fischer–Tropsch alkanes ($H_2/CO \sim 2$), methanol for dimethyl ether ($H_2/CO \sim 2$), or mixed alcohol fuel ($H_2/CO \sim 1.2$).[5]

Department of Chemical Engineering and Materials Science, University of Minnesota, 421 Washington Ave, Minneapolis, MN, 55455, USA. E-mail: schmi001@umn.edu; Fax: +1 612 626 7246

† Electronic supplementary information (ESI) available: The supplementary material contains a description of the assumptions that went into the construction of Fig. 7. See DOI: 10.1039/b804691c

An extremely short residence time (milliseconds) reactor integrating at least three process steps provides the possibility for dramatic improvement in the utilization of biomass for synthetic fuels. Conventional gasifiers exhibit residence times on the order of seconds to minutes, while catalytic partial oxidation of organic compounds occurs in milliseconds permitting a reduction in biomass reactor size by at least an order of magnitude. Additionally, combined chemistries permit simpler overall processes by eliminating multiple process vessels and ancillary equipment. The capital costs of traditional BTL equipment has restricted the processes to large scales (~400 MW_{th}), demanding an abundant, local supply of biomass.[7] Small efficient processes allow for localized processing facilities, reducing costs associated with biomass transportation.

A highly integrated, millisecond biomass reactor operates faster and with more functionality than a large number of existing catalytic gasifiers. There exist numerous experimental examples of the integration of metal catalysts such as Ni, Co, and Rh with conventional fluidized bed gasifiers to reduce the production of char and tars *in situ*.[10–12] Most gasification catalysts exhibit deactivation and poisoning due to the development of surface carbon (coke) and char and the condensation of inorganic ash. Rh-based catalysts with the addition of Ce have exhibited significant resistance to the formation of coke in the oxidative reforming of tars and organics.[13,14] Additionally, catalytic partial oxidation of highly oxygenated organic compounds such as ethylene glycol and glycerol on Rh–Ce catalysts has selected for equilibrium concentrations of synthesis gas during steady, autothermal operation on millisecond time-scales.[15] The utilization of Rh–Ce fluidized catalytic beds integrated with volatilization of carbohydrate-rich solids has demonstrated reduced tar formation, but has been restricted to indirectly heated processes and residence times on the order of one second.[16]

The direct impingement of solid particles of carbohydrate-rich biomass with a hot (T > 700 °C), catalytic surface in thermal contact with a catalytic bed provides an optimal situation for fast, integrated processing of nonvolatile feedstock material. We have recently demonstrated this technique, referred to as 'reactive flash volatilization,' on Rh–Ce catalytic beds for the air-blown reforming of soy oil, cellulose, and lignocellulose.[17,18] Multiple zones of chemistry (volatilization, oxidation, and reforming) provide efficient chemical routes to synthesis gas. Particles contacting a hot surface volatilize to gases and volatile organic compounds (VOCs) which can flow into the catalyst bed and oxidize to synthesis gas and combustion species. The remaining gases and VOCs after >99% oxygen conversion can then steam reform to gases and equilibrate by the water-gas-shift (WGS) reaction. Autothermal processing is realized between endothermic zones (volatilization and reforming) and the exothermic oxidation chemistry through balanced heat transfer by conduction in the alumina catalyst support and convection forward by the process gases.

The adjustment of chemistry and heat transfer by the addition of steam and removal of feed N_2 provides the opportunity to reduce effluent synthesis gas dilution and fully integrate the water-gas-shift step within the millisecond reactor. Rh–Ce catalysts have demonstrated strong activity for the water-gas-shift reaction on millisecond time-scales.[19] In this study we demonstrate the tunability of the synthesis gas ratio by adjusting the feed S/C (steam-to-carbon) ratio, the C/O (carbon-to-oxygen) ratio, the N_2/O_2 (feed nitrogen/feed oxygen) ratio, and the total flow rate of solid material. Spatial temperature measurements were conducted along the axis of the catalyst bed to analyze system behavior and define process limitations. Additionally, system performance is analyzed through thermodynamic analysis, and the domain of operation is presented for considered feed parameters. Finally, the results lead to the development of an autothermal, steady-state operating configuration that permits integration of gasification, tar-cleaning, and water-gas-shift chemistry in the absence of nitrogen at high process feed rates and millisecond residence times.

Experimental

Reactor design

The autothermal steam reforming of cellulose was performed in a 20 mm I.D., 22 mm O.D. quartz tube shown in Fig. 1. A 17 mm O.D. ceramic foam monolith, used to support the 30 mm bed of

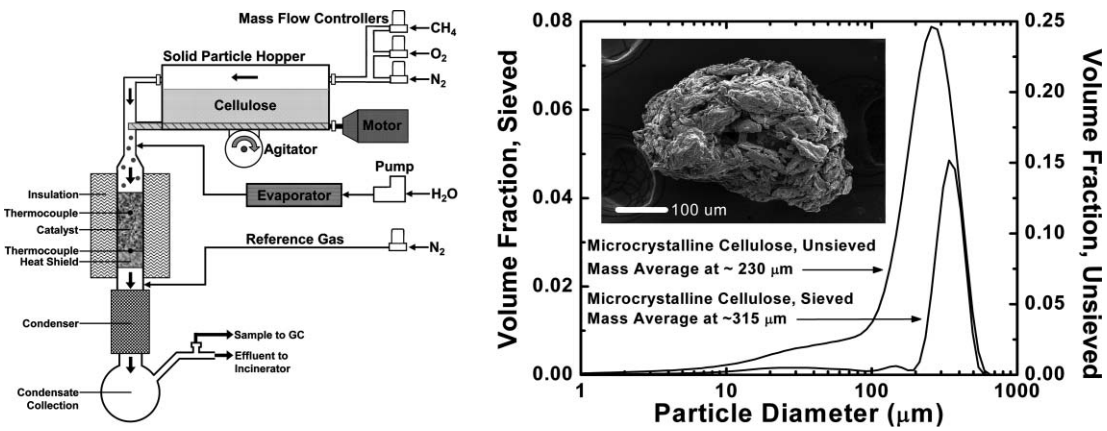

Fig. 1 Left: the experimental apparatus consisted of an insulated quartz reactor tube supplied with N_2, O_2, CH_4, cellulose, or steam. Particles of cellulose were metered using a servo-motor powered auger passing through a sealed hopper. Reactor effluent gases passed through a condenser and were sampled for gas chromatography. Right: particle size distribution generated by light scattering of microcrystalline cellulose samples processed by reactive flash volatilization. Inlet micrograph shows a representative cellulose reactor feed particle with high porosity.

spherical catalysts, was inserted into the quartz tube from the bottom and held in place *via* friction fit against the reactor wall with ceramic cloth.

Cellulose was fed to the top of the reactor tube with a 0.25 in. auger, which was rotated by a small volume laboratory mixer to accuracies ±1 RPM. The auger functioned as a volumetric feeder, conveying cellulose from a gas-sealed acrylic hopper to the reactor. An unbalanced rotor vibrator was attached to the base of the hopper to ensure uniform and complete filling of the auger during operation, minimizing oscillation in fuel flow rates. Gases were fed through the hopper to the reactor using mass flow controllers operated by LabVIEW software accurate to ±0.05 SLPM. Water was supplied by a syringe pump to a steam generator, where it was vaporized and fed ~2 in. upstream of the catalyst bed *via* heated stainless steel tubing. Steam was fed in close proximity to the catalyst in order to avoid water condensation on the reactor walls and cellulose conglomeration prior to contact with the catalyst. The reactor effluent was directed through a laboratory condenser (maintained at 25 °C) to minimize throughput of condensable species, primarily water, to the sampling tube. Effluent was periodically sampled upstream of the condenser to verify the absence of condensable organic compounds.

Temperature measurement

Experiments were primarily conducted with thermocouples placed at 10 mm and 30 mm from the front face of the catalyst bed. These thermocouples were inserted from the downstream side of the reactor tube during the placement of the foam monolith support. Axial temperature profile experiments were conducted using a reactor tube with 16, 0.7 mm diameter holes placed in the quartz reactor tube along the length of the catalyst bed. Through these holes 16 K-type thermocouples were fed horizontally to the center of the catalyst bed as depicted in Fig. 5D. The quartz reactor tube was sealed using ultra high temperature ceramic adhesive. This apparatus facilitated the acquisition of steady state and transient reactor bed temperature profiles.

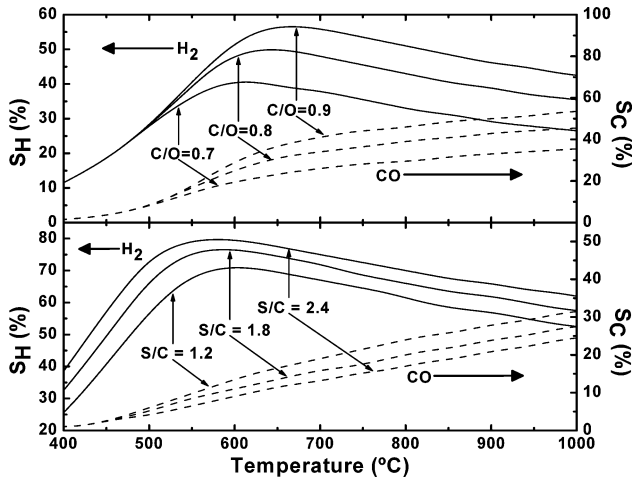

Fig. 2 The conversion of cellulose $(C_6H_{10}O_5)_n$ to equilibrium products by dry oxidation (upper panel) at C/O = 0.7, 0.8 and 0.9, and steam reforming at C/O = 0.8 (lower panel) at S/C = 1.2, 1.8 and 2.4, predicts 40–80% selectivity to H_2 (solid lines) and 0–50% selectivity to CO (dashed lines) for the temperature range 400–1000 °C. C/O is defined as molar feed rate of carbon in the fuel relative to molar feed rate of oxygen atoms in the gaseous O_2. S/C is defined as molar feed rate of steam relative to the molar feed fate of carbon in the fuel.

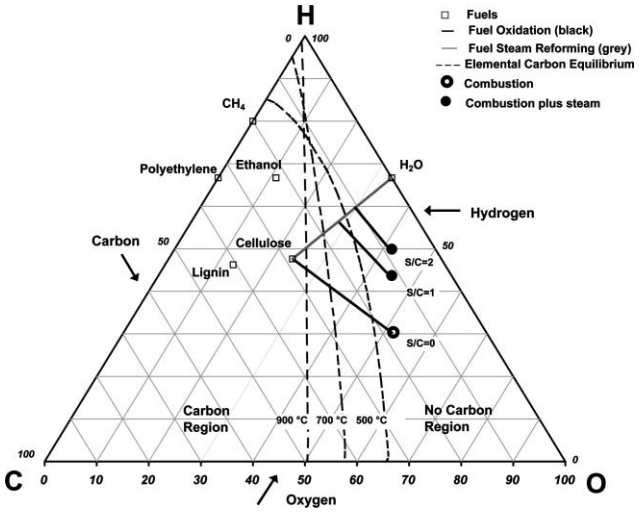

Fig. 3 The formation of solid carbon, C_S, by processing of solid, organic feedstocks such as cellulose, lignin, polyethylene, or ethanol inhibits the use of catalysts due to surface poisoning. Dashed lines represent the interface between the region for which C_S is predicted as a thermodynamic product, and the region for which it is not, at 500, 700, and 900 °C. The stoichiometry of steam reforming (solid grey line) cellulose oxidation and authothermal steam reforming (solid black lines) demonstrate that conversion to combustion products or synthesis gas occurs near the interface of these two regions permitting autothermal carbon-free processing.

Reactor operation

Reactor start-up involved pre-heating an isolated portion of the catalyst to ~300 °C using an external heat source while passing methane and nitrogen gas through the reactor. Once hot, oxygen was added to the gas mixture at air stoichiometry and fuel-rich conditions necessary to avoid combustion. This procedure initiated the autothermal partial oxidation of methane in the catalyst bed, which heated the reactor bed to ~900 °C. Cellulose was then added to the reactor at ~30 g h^{-1}. Flow of methane was discontinued, and the oxygen flow rate was adjusted to a fuel-rich regime for experimental trials.

The reactor was insulated to minimize heat loss to the surroundings. In order to accurately determine cellulose flow rate to the reactor, the system was initially operated at low C/O in order to heavily oxidize any carbon before being exhausted from the sphere bed. The effluent was then analyzed to quantify carbon content (*i.e.* the CO and CO_2 were measured with gas chromatography). Once a steady cellulose flow rate was observed, gases were adjusted to achieve the desired S/C, N_2/O_2, and C/O ratios, and the effluent was sampled. The system was then returned to a low C/O in order to verify that the cellulose flow rate had not changed. This procedure was used for determining the cellulose flow rate upon start-up, and for data obtained at operating conditions capable of producing condensable product species. The reactor was shut down by

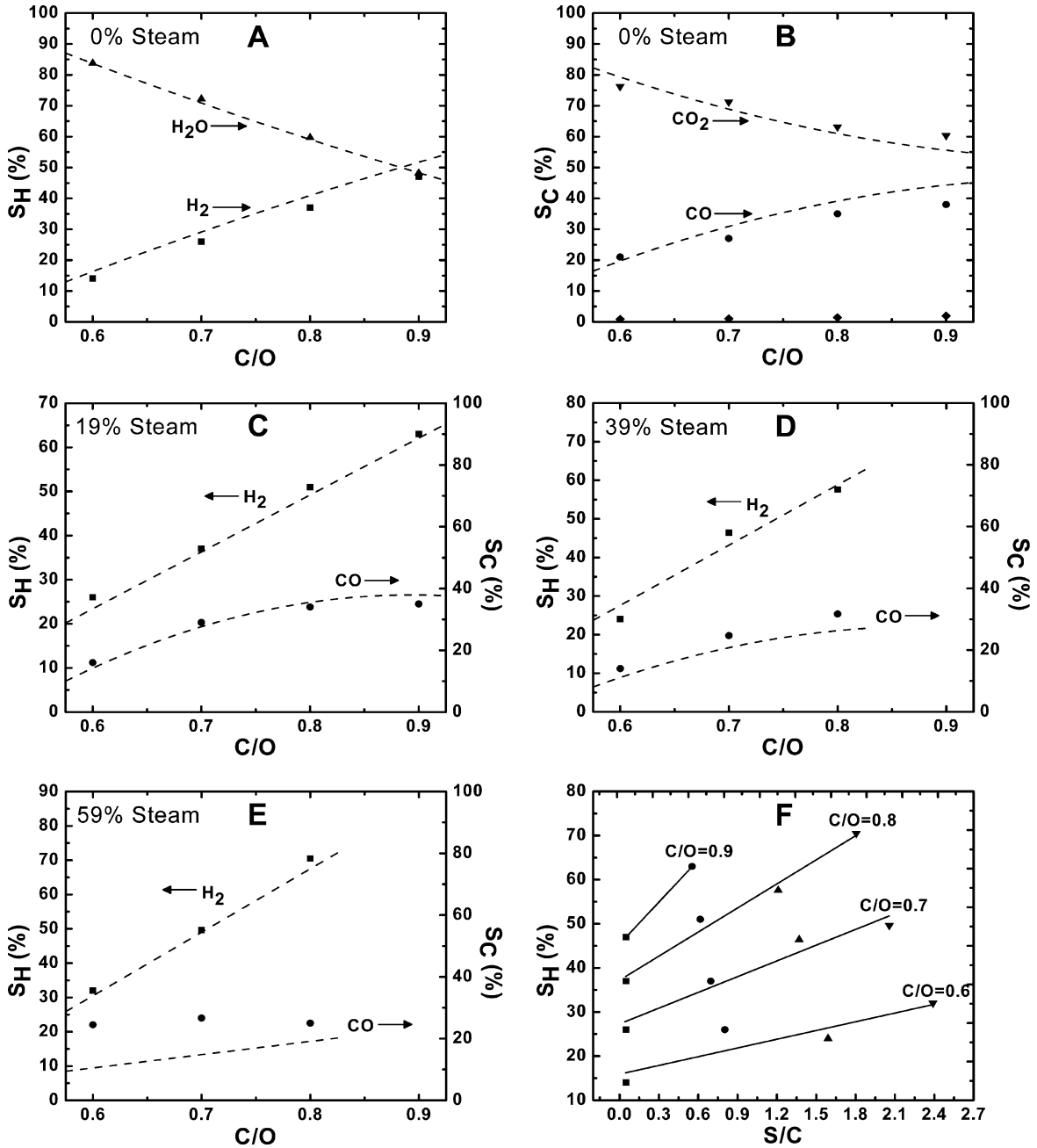

Fig. 4 The selectivity to hydrogen (■), water (▲), carbon monoxide (●), carbon dioxide (▼) and methane (◆) achieves equilibrium in the reforming of cellulose at a flow rate 30 g h^{-1} with gaseous co-feed: (79% N_2 + 21% O_2) in Panels A and B, co-feed (60% N_2 + 21% O_2 + 19% H_2O) in Panel C, co-feed (40% N_2 + 21% O_2 + 39% H_2O) in Panel D, co-feed (20% N_2 + 21% O_2 + 59% H_2O) in Panel E, and at $0 \leq S/C \leq 2.4$ in Panel F. Dashed lines represent equilibrium concentrations and solid lines are fitted.

terminating cellulose, oxygen, and steam flows. Once the system was cooled, nitrogen flow was terminated.

All experiments without steam addition were operated at air stoichiometry ($N_2/O_2 = 3.76$). C/O is defined to be the molar ratio of carbon in the fuel to atomic oxygen fed as air. Complete cellulose combustion to CO_2 and H_2O therefore occurs at C/O = 0.5. Experiments were carried out at C/O ratios of 0.6, 0.7, 0.8, and 0.9. These experiments were run in oxygen deficient environments in order to maximize selectivity to synthesis gas and hydrogen. Cellulose flow rates of 25–60 g h^{-1} were used for all data collection.

Steam addition experiments were performed by replacing nitrogen with steam in increments of 20% of the gaseous feed to maintain a constant gaseous co-feed flow rate. Gas feed compositions considered were (in mole percents): (1) 60% N_2, 21% O_2, 19% H_2O, (2) 40% N_2, 21% O_2, 39% H_2O, (3) 20% N_2, 21% O_2, 59% H_2O, and (4) 0% N_2, 21% O_2, 79% H_2O. S/C is defined to be the molar ratio of steam to carbon in the fuel.

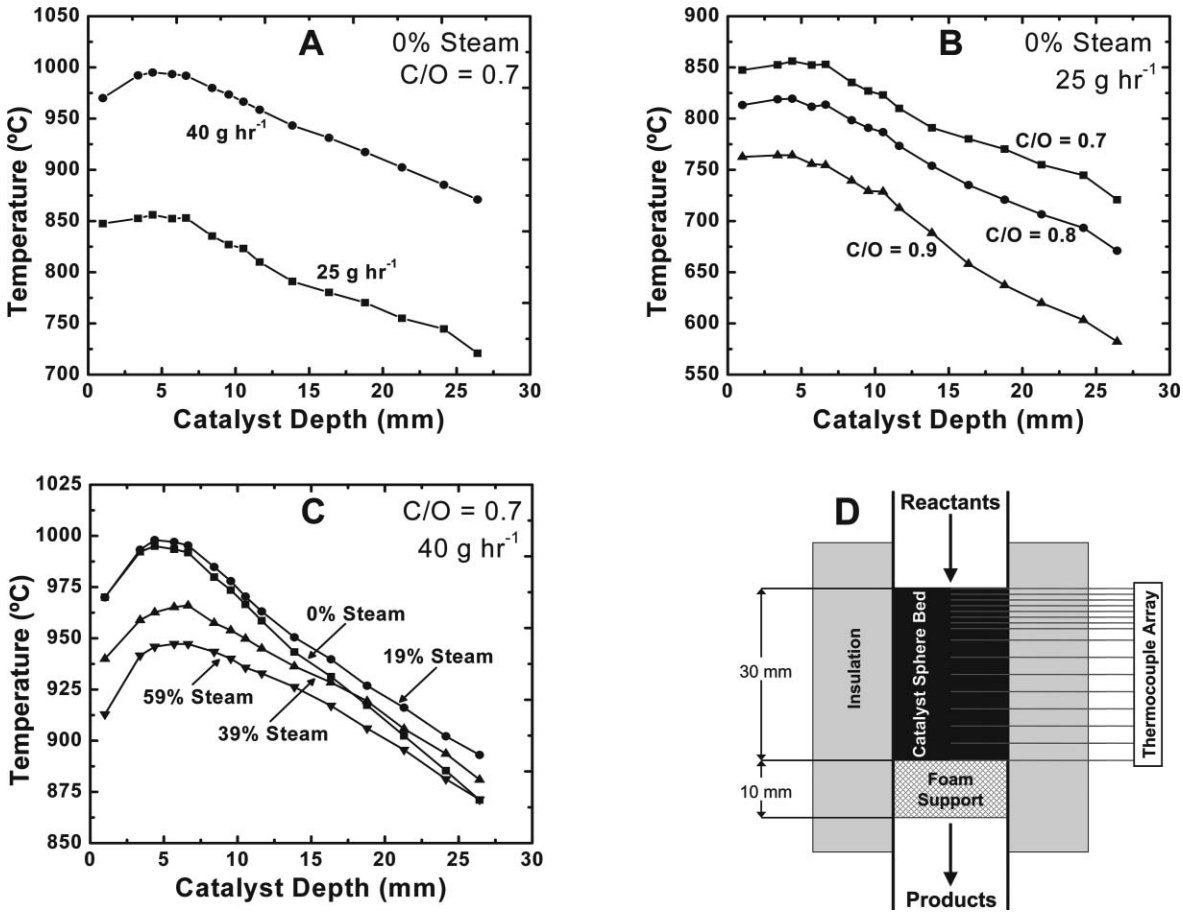

Fig. 5 Measured axial temperature profile within the 30 mm fixed bed of Rh–Ce/γ-Al_2O_3/α-Al_2O_3 spheres was examined as a function of total solid cellulose particle flow rate (A), C/O ratio (B), and magnitude of steam substitution for nitrogen (C). In Panel A, the temperature profile was measured with C/O = 0.7, S/C = 0.05, and at cellulose flow rates of 25 g h^{-1} (▼) and 40 g h^{-1} (●). In Panel B, the temperature profile was measured at S/C = 0.05, cellulose flow rate of 25 g h^{-1}, and C/O = 0.7 (■), C/O = 0.8 (●), and C/O = 0.9 (▲). In Panel C, the temperature profile was measured at a cellulose flow rate of 40 g h^{-1}, C/O = 0.7, and steam substitution of N_2 with steam in the gaseous feed of 0 mol% (■), 19 mol% (●), 39 mol% (▲), and 59 mol% (▼). The temperature at each axial position (catalyst depth) was measured simultaneously by inserting and sealing multiple thermocouples radially into the reactor (D).

Experiments were run at C/O ranging from 0.6 to 0.9, depending on whether autothermal operation was sustainable.

Catalyst preparation

All catalysts were prepared on Saint-Gobain NorPro Corporation 1.3 mm diameter α-Al_2O_3 spheres. The unmodified spheres have a surface area of 5.35 m^2 g^{-1} and a packing density of 64.1 lbs ft^{-3}. Prior to Rh–Ce deposition, a γ-Al_2O_3 washcoat was added to the spheres to increase surface area *via* incipient wetness technique.[20] A 5 wt% slurry of γ-Al_2O_3 in distilled water was added drop-wise to the spheres, which were then allowed to dry. Once dry, the spheres were calcined for 6 h at 600 °C. $Rh(NO_3)_3$ and $Ce(NO_3)_3 \cdot 6H_2O$ metal salts were then added to the spheres also using the incipient wetness technique. A 1 wt% Rh and 1 wt% Ce solution of metal salts in distilled water was added drop-wise to the spheres, which were then allowed to dry. Once dry, the spheres were calcined for 6 h at 600 °C. Catalysts were conditioned for ~1 h under representative operating conditions before conducting experiments. Experiments were repeated on catalysts with no measurable differences in activity. Catalysts were generally used for no less than 10 h, during which there was no observable deactivation.

Feedstock analysis

Microcrystalline cellulose used in all experiments was obtained from FMC BioPolymer. Samples of cellulose exposed to the air naturally absorbed ~5 wt% moisture (S/C~0.05). Moisture content was determined gravimetrically by drying in a vacuum oven. The particle size distribution in Fig. 1 was measured by light scattering. The raw cellulose sample was separated in a No. 50 mesh sieve to obtain a sample with fewer particles smaller than 200 μm to increase ease of handling by reducing particle conglomeration. Steam was produced from distilled water. The high purity gases, N_2 and O_2, were supplied separately with high pressure cylinders.

Product analysis

Gas samples were sampled with a syringe downstream of the condenser, and injected into a gas chromatograph. The system was calibrated to measure permanent gases and higher

hydrocarbon species. Species response factors and column retention times were determined using known concentrations of premixed gases. During standard operation the carbon, oxygen, and hydrogen mass balances typically closed to within ±5%.

Experiments were conducted several times, typically repeated on several identical catalysts, with no significant differences observed between experiments. Catalyst operating temperature and time ranged from 550–1100 °C and 10–30 h, respectively. Selectivity to product species was calculated on an atomic carbon basis, S_C(species), or an atomic hydrogen basis, S_H(species). The selectivity was defined as (atoms in the product species)/(atoms in the converted fuel). Co-fed steam was not considered fuel. The sum of all selectivities to product species based on the same element (C or H) should equal unity within experimental error. The residence time was calculated as the void volume of the catalyst bed divided by the volumetric flow of effluent gases at the exit temperature. Sphere beds exhibit smaller void fractions resulting in faster residence times than foams.

Equilibrium calculations

Equilibrium calculations were performed by numerical minimization of Gibbs free energy using HSC Chemistry® software.[21] Calculations were performed at 1 atm pressure and the temperature of the sphere bed 10 mm downstream of the front face (T_{10}). Back-face catalyst bed temperatures were not used due to significant temperature gradients, resulting from heat conduction to the monolith support. High (>99%) conversion of fuel to C_1 products was expected at low S/C, facilitating the inclusion of the following species in the calculation: CO_2, CO, CH_4, O_2, H_2, H_2O.

The measured reactor process efficiency in Table 1 has been examined by calculating the fuel chemical flow availability (exergy), a_i, of all non-cellulose species by eqn (1),

$$a_i = (h_i - h^\circ_i) - T^\circ(s_i - s^\circ_i) + (\mu^\circ_i - \mu_i) \quad (1)$$

where h_i is the specific enthalpy of the species i, T is the temperature, s_i is the specific entropy of species i, and μ_i is the chemical potential of species i.[22] The values of h°_i, s°_i, and μ°_i were calculated at the restricted dead state defined as T° = 298 K, P° = 1 atm, and the gaseous molar fractions X(O_2) = 0.20, X(N_2) = 0.76, X(H_2O) = 0.03, and X(other) = 0.01. The chemical availability of cellulose was calculated using a correlation developed by Szargut and Styrylska,

$$\beta = \frac{1.0438 + 0.1882\left(\frac{H}{C}\right) - 0.2509\left(\frac{O}{C}\right)\left(1 + 0.7256\frac{H}{C}\right)}{1 - 0.3035\frac{O}{C}} \quad (2)$$

where H, C, and O represent atomic mass fractions of feedstock cellulose, and β relates the chemical availability of cellulose, a_{cell}, to the lower heating value (LHV) of cellulose by $a_{cell} = \beta$*$LHV_{(cellulose)}$.[23] The lower heating value of cellulose, obtained from a correlation assuming C/H/O = 6/10/5, was 15.7 kJ g^{-1}.[24] Process efficiency in Table 1 is defined as the flow availability of all products divided by the flow availability of all feed species.

Results and discussion

The results demonstrate that reforming of cellulose with steam addition can produce equilibrium selectivity to synthesis gas with very little selectivity to minor products. By this method, the effluent syngas stoichiometry is tunable by adjusting the S/C ratio. Sustainable processing to a clean product stream maintains a significant fraction of the cellulose fuel value without observable formation of a solid carbon byproduct.

Table 1 Selected experimental data for the millisecond reforming of microcrystalline cellulose[a]

Experiment	1	2	3	4	5
Catalyst bed length/mm	30	30	30	30	60
C/O ratio	0.9	0.9	0.8	0.8	0.9
H_2O substitution for N_2	0	19	39	59	79
S/C ratio	0.05	0.55	1.21	1.81	2.14
N_2/O_2 ratio	3.76	2.86	1.91	0.95	0
Mass flow/g h^{-1}	30	30	30	30	60
Residence time/ms	33	31	24	25	29
Space velocity/mol h^{-1} L^{-1}	118	118	118	118	118
Mass velocity/h^{-1}	53	53	53	53	53
H selectivity (%)					
H_2	48	63	58	71	79
H_2O	38	34	42	21	21
C selectivity (%)					
CO	38	35	32	25	27
CO_2	60	64	68	72	72
CH_4	1.9	1.2	0.3	3	0.2
Temperature at 30/°C	600	730	710	625	825
H_2/CO	1.1	1.4	1.5	3.0	2.3
Syngas dry mole fraction (%)	18	24	22	25	42
Process efficiency (%)	58	66	63	68	73

[a] All experiments were considered on a bed of 1.3 mm α-Al_2O_3 spheres with 5 wt% γ-Al_2O_3 washcoat and 2 wt% loading of Rh and Ce with >99% conversion of cellulose to C_1 products. The space velocity was defined as (molar flow of carbon)/(volume occupied by the catalytic spheres). The mass velocity was defined as the (mass flow of carbon)/(mass of RhCe). The process efficiency was defined in the experimental section of the text.

Thermodynamic considerations

Fig. 2 shows representative equilibrium selectivity output data for the reaction of cellulose ($C_6H_{10}O_5$) with steam and oxygen at variable C/O and S/C. As the reaction feed becomes more carbon rich (increasing C/O), the selectivity to more oxygen deficient species such as $S_H(H_2)$ and $S_C(CO)$ increase. Additionally, as the reaction feed contains more steam (higher S/C), the selectivity to hydrogen, $S_H(H_2)$, increases and $S_C(CO)$ decreases. This behavior can be described very generally by an increased reaction of CO with steam to form hydrogen by the water-gas-shift reaction (WGS) (eqn (3)) at higher S/C.

$$\text{WGS: } CO + H_2O \leftrightarrow CO_2 + H_2,\ \Delta H^\circ = -41\ \text{kJ mol}^{-1} \qquad (3)$$

The gaseous products predicted in Fig. 2 are achievable, provided a chemical route exists to equilibrium. The formation of a second, solid phase of carbon, C_S, has the potential to develop on catalytic surfaces, blocking surface chemistry and preventing the reactor from operating sustainably. This inhibition can likely be eliminated if solid carbon or carbon-rich solid residue is not a favored thermodynamic product. The prediction of a solid carbon equilibrium product (C_S) is a function of the reaction feed stoichiometry (cellulose/oxygen/steam) and the reaction temperature. By calculating the stoichiometry for a set of temperatures (500, 700, and 900 °C) for which the activity of C_S goes to one, it is possible to define a boundary between a region for which C_S is unstable and not predicted by equilibrium. As shown in the ternary diagram of Fig. 3, this "no carbon region" is defined by a boundary (dashed lines) for which an increase in process temperature expands the operable "no carbon region" to nearly half of the possible reaction stoichiometry.[25,26]

The relevance of this calculation to the processing of feedstocks can be determined by placing the internal atomic stoichiometry (*i.e.* cellulose: C/H/O~28.6/47.6/23.8 mol%) of each material on the ternary diagram (points). All considered feedstocks exist within the region for which solid carbon is a predicted thermodynamic product at $T < 900$ °C. However, the addition of oxygen (solid black line) shifts the overall atomic stoichiometry across temperature boundaries such that no carbon is predicted at combustion stoichiometry (◎). Processing at oxygen-deficient (syngas-producing) conditions occurs along the cellulose oxidation line and at lower adiabatic temperatures than combustion. The key implication for autothermal reforming is that there exists a specific oxidation feed stoichiometry around C/O = 1.1 (C/O calculated as defined in the experimental section) for the considered reaction conditions for which carbon becomes a predicted product. The addition of steam provides a processing alternative (solid grey line) to extend the overall stoichiometry across the thermodynamic boundaries. By co-feeding steam with oxygen at S/C = 1.0, nearly the entire oxidation stoichiometry exists within the no-carbon region defined at 500 °C, and higher S/C offer and even more expansive range of feed stoichiometry.

Autothermal catalytic partial oxidation of cellulose

The production of gaseous products from the autothermal reforming of cellulose at S/C = 0.05 (due to particle moisture) is described in panels A and B of Fig. 4. Steady operation was observed at all experimental conditions without oxygen breakthrough, and transient behavior due to a change in experimental operating conditions was resolved in 1–2 min. Carbon conversion to C_1 products is >99% for all C/O presented, and carbon selectivity to methane was <3% for all C/O. Selectivity to H_2 ranges from a minimum of 14% at C/O = 0.6, to a maximum of 47% at C/O = 0.9. The majority of the remaining hydrogen atoms were converted to water. Selectivity to carbon monoxide ranges from a minimum of 21% at C/O = 0.6, to a maximum of 38% at C/O = 0.9. The majority of the remaining carbon atoms were converted to CO_2. For C/O < 1.0 at S/C = 0.05, experimentally measured selectivity to gaseous products achieved equilibrium within experimental error. Complete conversion was attainable at residence times less than 40 ms.

At C/O = 1.0, production of organic species larger than C_1 was observed in the chromatogram. The incomplete decomposition to equilibrium products can be attributed to slower kinetics, resulting from the decreased temperature at C/O = 1.0. For all C/O, the coldest part of the catalyst bed (T_{30}) never dropped below 500 °C. The experimentally measured temperatures are shown in Fig. 5, and will be discussed in the next section. Overall performance with alumina spheres as a support for the Rh–Ce catalyst was very similar to that of 80 ppi alumina foams.[17]

Panels C–E of Fig. 4 show selectivity to hydrogen and carbon monoxide as a function of C/O for the CPO*x* of cellulose at varying concentrations of N_2, O_2, and H_2O feed gases. Steady operation was observed at all experimental conditions without oxygen breakthrough, and transient behavior due to a change in experimental operating conditions was resolved in 1–2 min. Carbon conversion to C_1 products is >99% for all C/O presented. Additionally, average methane selectivity with respect to carbon was <3% for all C/O. In panel C, 19% molar substitution of nitrogen with steam raised the selectivity to H_2 to 63% while lowering selectivity to CO to 35% at C/O = 0.9. When the substitution for nitrogen with steam was raised to 39% in panel D, the overall operating temperature decreased (shown in Fig. 5), and the C_2 organic species were observed at C/O = 0.90. However, at C/O = 0.8, selectivity to H_2 was 58% and selectivity to CO was 32%. Further substitution of steam for nitrogen to 59% H_2O gaseous feed further cooled the operating temperature of the reactor (Fig. 5), but the addition of steam raised the observed selectivity of H_2 to 71% and lowered the selectivity to CO to 25% at C/O = 0.8. Panel F of Fig. 4 relates the observed species to the operating S/C ratio for each of the experimental trials.

Spatial temperature profiles

Measurements of the temperature within the fixed bed of catalyst spheres provide experimental insight to support the proposed mechanism detailed in the next section. By inserting thermocouples radially into the fixed bed of catalyst as shown in panel D of Fig. 5, the temperature at which reforming chemistry is occurring is known with millimetre resolution. Panels A, B, and C describe the effect of cellulose flow rate, process C/O ratio, and magnitude of steam substitution for nitrogen, respectively.

Panel A of Fig. 5 shows that the spatial temperature profile is a very strong function of the flow rate of cellulose. Both flow rates,

25 g h^{-1} and 40 g h^{-1}, exhibit a rise in temperature between the top of the catalyst bed (0 mm) and the maximum temperature (~5 mm). However, the magnitude of the temperature increase appears to be a function of the total flow rate with higher feedstock flow rates exhibiting higher thermal gradients within the oxidation zone. This can be partially explained by an increased distance between the endothermic chemistry at the catalyst front face and exothermic chemistry taking place in the oxidation zone. In contrast, both flow rates of cellulose exhibit the same rate of temperature decline after the temperature maximum (~5–30 mm). The difference in exit temperature (T_{30}) for differing flow rates can be attributed to heat loss from the reactor.

Panel B of Fig. 5 details the effect of C/O ratio on the spatial temperature profile for a cellulose feed rate of 25 g h^{-1} at S/C = 0. More oxygen feed (lower C/O) exhibits an overall hotter profile due to more overall exothermic chemistry. Panel C of Fig. 5 shows the effect of substituting steam for nitrogen at 0 mol%, 19 mol%, 39 mol%, and 59 mol% on the spatial temperature profile for a cellulose feed rate of 40 g h^{-1} and C/O = 0.7. The initial substitution (0→19 mol%) has the effect of slightly raising the temperature from ~5–30 mm likely due to the temperature of steam (100 °C). However, further substitution (19→39 mol%, and 39→59 mol%) monotonically decreases the overall temperature profile 10–15 °C. A likely explanation is the increased heat capacity of steam over nitrogen.

Process chemistry

The process by which solid particles of cellulose ~315 μm in average diameter are reduced to C_1 products (Fig. 6) at millisecond time scales must account for particle volatilization in the presence of oxygen integrated with the catalytic partial oxidation of volatilized products on a noble metal surface. Each process (particle volatilization or catalytic reforming) consists of complex multi-phase chemical mechanisms and multiple modes of heat transfer for which the current understanding by computer modeling does not even extend to the individual process.[27,28] The chemical and heat integration of the two processes expands the complexity of the overall reaction such that mechanistic observations are currently only available through effluent data and experiments considering more simple fuel species.

The impact of the cellulosic particle with the hot catalytic surface likely initiates the process chemistry. The extent of particle conversion occurring within the gaseous region 3–10 mm above the catalytic bed is likely limited, because previous examination has measured the gas-phase temperature of this region less than 300 °C severely limiting particle conversion by pyrolysis.[17,29] Fig. 5 (panel B) shows that T = 700–800 °C for C/O = 0.9 at the leading edge of the catalyst, providing sufficient conductive heat transfer from catalyst support to particle for volatilization.

Particle volatilization is likely a complex convolution of heat transfer and reaction chemistry. Complete particle conversion must account for at least (1) the drying of the particle (~5 wt% moisture), (2) cellulose pyrolysis to gases (*e.g.* CO, H_2), volatile organics, and chars, (3) volatile organic cracking to gases, and (4) oxidation of gases, volatile organics, and chars. Multiple cellulose pyrolysis lumped kinetic models exhibit some form of competitive pathways to either gases (*e.g.* H_2O) and char, volatile organics (*e.g.* acetic acid, methanol), or just gases.[30–34] Fluidized bed fast pyrolysis reactors maximize selectivity (~70 wt%) to volatile organics around 500 °C for ~1–2 s with millimetre-sized particles.[35] Lower temperatures favor char production, while higher temperatures exhibit higher selectivity to gases with the lower kinetic limit for char production of ~3 wt% at 700–800 °C.[36]

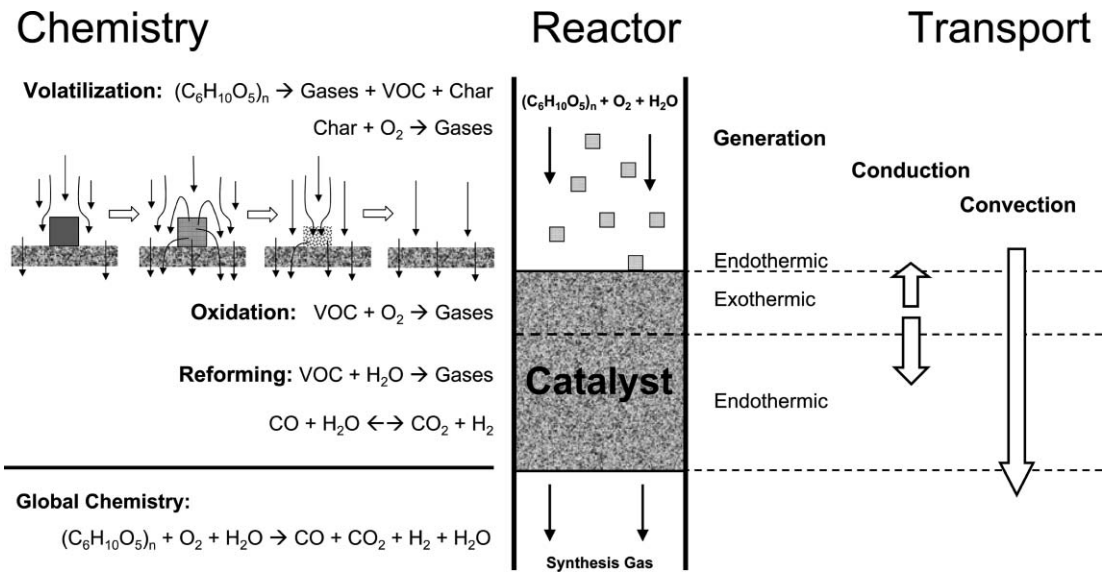

Fig. 6 The proposed chemical and thermal integration of millisecond particle reforming on a fixed bed of noble metal catalyst permits rapid conversion of organic solid materials to synthesis gas. Particles undergo rapid endothermic volatilization upon impact with a hot, catalytic surface, producing gases (*e.g.* H_2 and CO) and volatile organic compounds (VOCs). Volatile species flow into the catalyst and produce gases by exothermic surface and gaseous oxidation chemistry. Thermal energy generated in the oxidation zone conducts upward to the volatilization zone, and down to the reforming zone where remaining VOCs and gases undergo steam reforming and water-gas-shift to achieve equilibrium selectivity to synthesis gas.

Application of cellulose pyrolysis kinetics to spherical geometry to account for heat and mass transport has considered particle degradation in an inert atmosphere extensively.[37–39] Under optimal fast pyrolysis conditions, organic particles as large as 1 mm usually exhibit heat transport control, while particles with diameters less than ~200 μm exhibit chemical kinetic control.[37] The experiment considered here examines a related situation of direct impingement of a ~315 μm particle with a hot surface. One-dimensional transport/kinetic models considering solid cellulose rods contacting isothermal hot surfaces has shown superior selectivity to volatile organics due to higher particle heating rates.[36] In an inert atmosphere with solid surface temperatures of 700–800 °C, models predict cellulose pyrolysis of particles on the order of millimetres to exhibit selectivity to volatile organics as high as ~90 wt% and char less than 5 wt%.[40]

The applicability of these simulations to the particle volatilization of the considered experiment depends greatly on the magnitude of oxidation chemistry occurring within the particle by interaction with the gaseous feed. The considered microcrystalline cellulose, depicted in Fig. 1, exhibits high porosity permitting an initial internal supply of oxygen. However, the evolution of gases and volatile organics that must be transported to the particle surface due to a difference in density must significantly hinder diffusion of oxygen into the particle. Alternatively, the oxidation of evolved species at the particle surface can only be elucidated through the consideration of a flow boundary layer as has been considered for particle combustion in a methane flame.[27]

Evolved species from the solid particle likely mix with the bulk gas (O_2 + N_2 + H_2O) and flow into the fixed catalyst bed of Rh–Ce/γ-Al_2O_3/α-Al_2O_3 spheres. Likely devolatilized species include the same species observed in bio-oil samples that are derived from carbohydrate pyrolysis such as methanol, hydroxyacetaldehyde, acetic acid, or several furan-based compounds.[41] Highly oxygenated species such as polyols (ethylene glycol and glycerol) have exhibited continuous, steady-state processing to synthesis gas with high conversion (>99%) and equilibrium selectivity to synthesis gas.[15] Similar behavior has also been observed from the reforming of other species classes including esters and acids, ethers, and sugars.[18,42,43] However, the role of competition existing within mixtures for surface chemistry is unknown, and limited research exists examining the catalytic partial oxidation of mixtures of organics.[44]

The conversion of oxygenated species by catalytic partial oxidation is likely to occur by the general mechanism observed with methane reforming. Internal species measurements of methane have shown that conversion of fuel occurs in two distinct zones: oxidation and reforming.[45] In the oxidation zone, volatile fuel species premixed with bulk gases enter the fixed-bed of catalyst spheres at high velocity and undergo exothermic surface oxidation chemistry. Greater than 99% of oxygen is consumed (by definition) within this region likely producing a significant fraction of the thermodynamic species (H_2, H_2O, CO, and CO_2) by surface chemistry. At low C/O ratios (more oxygen rich), the oxidation zone converts a large fraction of the fuel.

At higher C/O, a more significant fraction of fuel passes through the oxidation zone to the reforming zone. Endothermic surface chemistry between fuel and oxidation products such as H_2O (steam reforming) or CO_2 (dry reforming) provide chemical routes to equilibrium. Additionally, the gas temperature is sufficiently high to permit endothermic cracking of fuel to smaller fuel species. Both of these chemistries are likely occurring simultaneously, effectively lowering both the surface and gas phase temperature as shown in Fig. 5. The performance of the reforming zone ultimately determines the conversion of volatile fuel species. By selecting a sphere bed (small pores) with a γ-Al_2O_3 washcoat, the reactor is tuned in favor of the surface chemistries to the desired C_1 species. For high conversion of fuel, this zone must remain sufficiently hot to permit chemistries at millisecond time-scales. As C/O increases, less thermal energy is generated in the oxidation zone, and the endothermic chemistry of the reforming zone critically cools denying complete conversion of volatile organics. By this mechanism, volatile organics are initially produced at C/O > 1.0 for fuel flow rates of 25–40 g h^{-1} on the considered fixed bed catalytic reactor (L = 30 mm).

Process limitations

The combination of solid conversion chemistry with the autothermal reforming of gaseous compounds introduces a greater number of process variables and prevents a clear definition of the limits of the process. If the objective of the process is steady long-term reforming to synthesis gas, then selected sets of process parameters which result in either incomplete conversion to C_1 products, catalyst deactivation, or upstream combustion of particles are outside of the domain of sustainable parameters. The incomplete conversion of cellulose to C_1 was observed when the temperature 30 mm into the catalyst bed was at or below about 500 °C. Table 1 (trials 1–4) lists a set of performance specifications that permit operation relatively close to this requirement. Catalyst deactivation can occur if the maximum in temperature observed at ~5 mm within the catalyst bed exceeds ~1200 °C, permitting conversion of γ-Al_2O_3 to α-Al_2O_3 or sintering of Rh. This high temperature is accessible at any flow rate (25–60 g h^{-1}) provided the C/O is low enough to generate sufficient heat. The third major process restriction is the ignition of solid particles above the catalyst which can propagate up the feed stream in an unsafe, unsustainable manner. The minimum ignition temperature of small (1 μm–1 mm) organic particles is a function of at least particle size and concentration, with smaller particles igniting at lower temperatures.[46] The precise characteristics describing the ignition of particles approaching a hot surface are unknown. However, we have demonstrated that sets of process parameters exist for which processing can occur without dilution with N_2 on particles as small as 300 μm.

Process performance

Using the knowledge gained from the experiments described in Fig. 4 and 5, experimental trials were executed to demonstrate the conversion of solid cellulose to an optimal synthesis gas stream. By selecting a fixed sphere-bed catalyst 6 cm in length and a process flow rate of 60 g h^{-1} at a C/O = 0.9 with steam addition of S/C = 2.14 and 0% nitrogen addition, it was possible to completely convert cellulose to a synthesis gas rich stream with a synthesis gas ratio of H_2/CO = 2.3 comprising a dry mole fraction of 42%. Under these conditions the reactor exhibited

steady autothermal reforming with no oxygen breakthrough at a gaseous residence time less than 30 ms. Additionally, ~80% of the atomic hydrogen provided by the feedstock cellulose was converted to molecular H_2.

Analysis of the conversion from a solid fuel to a gaseous fuel must account for the loss in fuel value. Using the method described in the experimental section, the maximum theoretical work that could be achieved from the feedstock cellulose (availability) was ~18 MJ kg^{-1}. By millisecond reforming, nearly ~75% of this potential was maintained as the gaseous effluent in the optimal experiment (trial 5 of Table 1). Most of the retained fuel availability existed within the synthesis gas (75–80%) with the remaining fraction occurring with the high temperature (600–800 °C) steam, carbon dioxide or nitrogen. The loss in ~25% of the fuel value of cellulose can be attributed process irreversibilities such as the generation of a large number of moles from cellulose. The primary benefit offsetting the one quarter loss in fuel value is an improvement in ease of fuel handling. Relative to gases, the transportation of solids within a chemical process remains a demanding, energy intensive technique requiring significant maintenance.

Comparison of the autothermal steam reforming of cellulose with other catalytic gasification techniques will ultimately determine the benefit of small, fast chemistry. While a complete process design and economic analysis is ultimately the best technique for determining the optimal process, an analysis of the operation of the gasification reactor provides an alternative metric that can be realistically assessed within this report. Fig. 7 details the performance of four different biomass gasification reactors containing multiple catalysts with the goal of relating the rate of biomass processing to both the size of the reactor and the use (mass) of the catalyst. The carbon space velocity has been defined as the ratio of the molar flow rate of biomass carbon to the volume necessary for reaction chemistry. By this definition, higher carbon space velocities result in smaller reactors. The carbon mass velocity has been defined as the ratio of the mass flow of biomass carbon to the mass of catalyst such that higher mass velocities result in lower use of catalyst. Full details of all data points and calculations are located in the electronic supplementary information.†

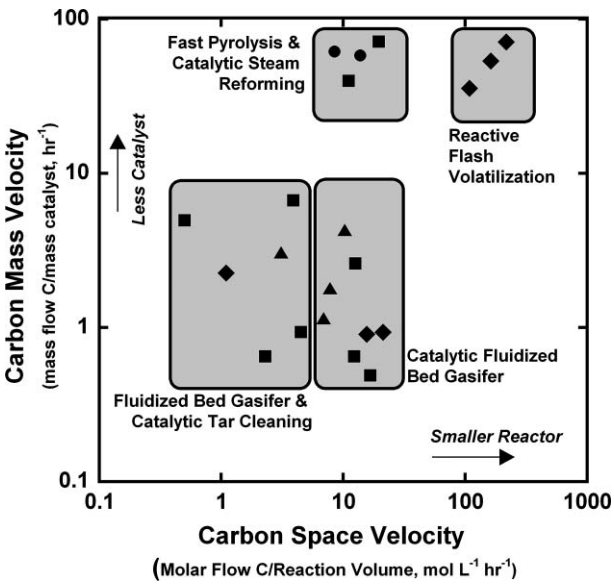

Fig. 7 Various processes to convert organic solids to synthesis gas exhibit operational performance grouped by process type despite utilizing several different catalysts: dolomite (▲), Ni (■), Rh (◆), Ru (●). The carbon space velocity provides a measure of the reactor volume by relating the molar processing of carbon to the volume necessary for chemical conversion. The carbon mass velocity provides a measure of catalyst usage by relating the molar processing of carbon to the mass of the catalyst. Complete details and references are located in the ESI.†

As shown in Fig. 7, the existing technology for the BTL process of fluidized (circulating and bubbling) bed gasifiers with downstream gas cleaning in fixed bed catalytic reactors exhibit carbon space velocities of ~0.5–8.0 mol L^{-1} h^{-1} and carbon mass velocities of ~0.8–9.0 h^{-1}. By applying catalysts directly to the fluidized bed, the use of catalyst (mass velocity) remains about the same, but the volume can be reduced as the space velocity increases to 8.0–30 mol L^{-1} h^{-1}. An alternative process to produce synthesis gas produces volatile organics (bio-oil) in fluidized bed reactors which can be steam reformed to synthesis gas. Because this process still uses a fluidized bed, the space velocity remains in the 8.0–30 mol L^{-1} h^{-1} range, but the high throughput of bio-oil steam reformers has permitted very high utilization of the Ni and Ru catalysts corresponding to high mass velocities in the range of 50–80 h^{-1}. Millisecond reactors further improve the carbon space velocity to 100–300 mol L^{-1} h^{-1} by carrying out the solid conversion to reformable species directly on the reforming catalyst. In general, millisecond reactors are at least an order of magnitude smaller and use less catalyst than most conventional catalytic gasification schemes.

Conclusions

We show that three sets of chemistries necessary for the biomass-to-liquids process (volatilization of cellulose, tar-cleaning of organic compounds, and the water-gas-shift of the gaseous effluent) can be integrated into one continuous flow catalytic reactor by reactive flash volatilization. Complete conversion of microcrystalline cellulose particles (~300 μm) to only C_1 products can occur faster than 30 milliseconds with the use of Rh–Ce/γ-Al_2O_3 catalysts over a wide range of S/C, C/O, and N_2/O_2. Steady, autothermal reforming without the presence of a diluent such as N_2 produces a more synthesis gas rich effluent. Additionally, the effluent synthesis gas ratio is tunable ($1.0 < H_2/CO < 3.0$) by manipulating the S/C of the reactor feed. The process appears to occur by the thermal integration of endothermic particle volatilization driven by heat conducted from an exothermic oxidation zone within the catalyst bed. Sufficient heat transfer from the oxidation zone to the entire fixed catalytic bed is thought to maintain the temperature above that at which coke is predicted by equilibrium. By this method, optimal processing conditions permit conversion such that ~75% of the fuel value of the cellulose is maintained in the synthesis gas effluent.

Acknowledgements

This work was supported by the U.S. Department of Energy (DOE), Office of Basic Energy Sciences and the Initiative for Renewable Energy (IREE) at the University of Minnesota–Twin Cities.

Notes and References

1 A. J. Ragauskas, *et al.*, The Path Forward for Biofuels and Biomaterials, *Science*, 2006, **311**, 484–489.
2 K. Sanderson, U.S. Biofuels: A Field in Ferment, *Nature*, 2006, **444**, 673–676.
3 R. D. Perlack, L. L. Wright, A. F. Turhollow, R. L. Graham, B. J. Stokes and D. C. Erbach, *Biomass as feedstock for a Bioenergy and Bioproducts Industry: The Technical Feasibility of a Billion-Ton Annual Supply*, United States Department of Energy, Oak Ridge National Laboratory, Oak ridge, Tn, USA, DOE/GO-102005-2135, 2005, pp. 1–78.
4 M. J. A. Tijmensen, A. P. C. Faaij, C. N. Hamelinck and M. R. M. van Hardeveld, Exploration of the possibilities for production of Fischer Tropsch liquids and power *via* biomass gasification, *Biomass Bioenergy*, 2002, **23**, 129–152.
5 S. Phillips, A. Aden, J. Jechura, D. Dayton and T. Eggeman, *Thermochemical Ethanol* via *Indirect Gasification and Mixed Alcohol Synthesis of Lignocellulosic Biomass*, U.S. Department of Energy, National Renewable Energy Laboratory, Golden, CO, USA, NREL/TP-510-41168, 2007, pp. 1–58.
6 J. R. Rostrup-Nielsen, Syngas in Perspective, *Catal. Today*, 2002, **71**, 243–247.
7 C. N. Hamelinck, A. P. C. Faaij, H. den Uil and H. Boerrigter, Production of FT transportation fuels from biomass; technical options, process analysis and optimization, and development potential, *Energy*, 2004, **29**, 1743–1771.
8 J. P. Ciferno, J. Marano, *Benchmarking Biomass Gasification Technologies for Fuels*, National Energy Technology Laboratory, US Department of Energy, Pittsburgh, PA, USA, 2002.
9 T. A. Milne, R. J. Evans, *Biomass Gasifier 'Tars': Their Nature, Formation, and Conversion*, U.S. Department of Energy, National Renewable Energy Laboratory, Golden, CO, USA, NREL/TP-570-25357, 1998, pp. 1–68.
10 K. Tomishige, M. Asadullah and K. Kunimori, Syngas production by biomass gasification using $Rh/CeO_2/SiO_2$ catalysts and fluidized bed reactor, *Catal. Today*, 2004, **89**, 389–403.
11 P. Lv, Z. Yuan, C. Wu, L. Ma, Y. Chen and N. Tsubaki, Bio-syngas production from biomass catalytic gasification, *Energy Convers. Manage.*, 2007, **48**, 1132–1139.
12 K. Tasaka, T. Furusawa and A. Tsutsumi, Biomass gasification in fluidized bed reactor with Co catalyst, *Chem. Eng. Sci.*, 2007, **62**, 5558–5563.
13 M. Asadullah, S. Ito, K. Kunimori, M. Yamada and K. Tomishige, Biomass gasification to hydrogen and syngas at low temperature: Novel catalytic system using fluidized-bed reactor, *J. Catal.*, 2002, **208**, 255–259.
14 K. Tomishige, T. Miyazawa, M. Asadullah, S. Ito and K. Kunimori, Catalyst performance in reforming of tar derived from biomass over noble metal catalysts, *Green Chem.*, 2003, **5**, 399–403.
15 P. J. Dauenhauer, J. R. Salge and L. D. Schmidt, Renewable hydrogen by autothermal steam reforming of volatile carbohydrates, *J. Catal.*, 2006, **244**, 238–247.
16 M. Asadullah, K. Tomishige and K. Fujimoto, A novel catalytic process for cellulose gasification to synthesis gas, *Catal. Commun.*, 2001, **2**, 63–68.
17 P. J. Dauenhauer, B. J. Dreyer, N. J. Degenstein and L. D. Schmidt, Millisecond reforming of solid biomass for sustainable fuels, *Angew. Chem., Int. Ed.*, 2007, **46**, 5864–5867.
18 J. R. Salge, B. J. Dreyer, P. J. Dauenhauer and L. D. Schmidt, Renewable hydrogen from nonvolatile fuels by reactive flash volatilization, *Science*, 2006, **314**, 801–804.
19 C. Wheeler, A. Jhalani, E. J. Klein, S. Tummala and L. D. Schmidt, The water-gas-shift reaction at short contact times, *J. Catal.*, 2004, **223**, 191–199.
20 A. S. Bodke, S. S. Bharadwaj and L. D. Schmidt, The Effect of Ceramic Supports on Partial Oxidation of Hydrocarbons over Noble Metal Coated Monoliths, *J. Catal.*, 1998, **179**(1), 138–149.
21 A. Roine, *Outokumpu HSC Chemistry for Windows Ver. 4.0*, Outokupu Research Oy, Pori, Finland, 2007.
22 M. J. Moran, *Availability Analysis: A Guide to Efficient Energy Use*, ASME Press, New York, 1989.
23 J. Szargut, T. Styrylska, Approximate evaluation of the exergy of fuels, Brennst, *Waerme Kraft*, **16**, 1964, pp. 589–596.
24 M. Dietenberger, Update for Combustion Properties of Wood Components, *Fire Mater.*, 2002, **26**, 255–267.
25 S R. F. Probstein and R. E. Hicks, *Synthetic Fuels*, Dover Publications Inc, Mineaola N. Y., 2006.
26 K. J. Ptasinski, M. J. Prins and A. Pierik, Exergetic evaluation of biomass gasification, *Energy*, 2007, **32**, 568–574.
27 Y. B. Yang, V. N. Sharifi, J. Swithenbank, L. Ma, L. I. Darvell, J. M. Jones, M. Pourkashanian and A. Williams, Combustion of a Single Particle of Biomass, *Energy Fuels*, 2008, **22**, 306–316.
28 A. B. Mhadeshwar and D. G. Vlachos, Hierarchical multiscale mechanism development for methane partial oxidation and reforming and for thermal decomposition of oxygenates on Rh, *J. Phys. Chem. B*, 2005, **109**, 16819–16835.
29 C. Di Blasi, Comparison of semi-global mechanisms for primary pyrolysis of lignocellulosic fuels, *J. Anal. Appl. Pyrolysis*, 1998, **47**, 43–64.
30 A. G. W. Bradbury, Y. Sakai and F. Shafizadeh, A Kinetic Model for Pyrolysis of Cellulose, *J. Appl. Polym. Sci.*, 1979, **23**, 3271–3280.
31 A. G. Liden, F. Berruti and D. S. Scott, A Kinetic Model for the Production of Liquids from the Flash Pyrolysis of Biomass, *Chem. Eng. Commun.*, 1988, **65**, 207–221.
32 J. P. Diebold, A Unified, Global Model for the Pyrolysis of Cellulose, *Biomass Bioenergy*, 1994, **7**, 75–85.
33 M. J. Antal, Jr. and G. Varhegyi, Cellulose Pyrolysis Kinetics: The Current State of Knowledge, *Ind. Eng. Chem. Res.*, 1995, **34**, 703–717.
34 J. G. Reynolds and A. K. Burnham, Pyrolysis Decomposition Kinetics of Cellulose-Based Materials by Constant Heating Rate Micropyrolysis, *Energy Fuels*, 1997, **11**, 88–97.
35 A. V. Bridgwater, Renewable fuels and chemicals by thermal processing of biomass, *Chem. Eng. J.*, 2003, **91**, 87–102.
36 C. Di Blasi, The state of the art of transport models for charring solid degradation, *Polym. Int.*, 2000, **49**, 1133–1146.
37 A. M. C. Janse, R. W. J. Westerhout and W. Prins, Modelling of flash pyrolysis of a single wood particle, *Chem. Eng. Process.*, 2000, **39**, 239–252.
38 D. R. Soravia and P. Canu, Kinetics modeling of cellulose fast pyrolysis in a flow reactor, *Ind. Eng. Chem. Res.*, 2002, **41**, 5990–6004.
39 L. J. Curtis and D. J. Miller, Transport model with Radiative Heat Transfer for Rapid Cellulose Pyrolysis, *Ind. Eng. Chem. Res.*, 1988, **27**, 1775–1783.
40 C. Di Blasi, Heat transfer mechanisms and multi-step kinetics in the ablative pyrolysis of cellulose, *Chem. Eng. Sci.*, 1996, **51**, 2211–2220.
41 M. Garcia-Perez, A. Chaala, H. Pakdel, D. Kretschmer and C. Roy, Characterization of bio-oils in chemical families, *Biomass Bioenergy*, 2007, **31**, 222–242.
42 D. C. Rennard, P. J. Dauenhauer and Sarah A. Tupy, Autothermal Catalytic Partial Oxidation of Bio-Oil Functional Groups: Esters and Acids, *Energy Fuels*, 2008, **22**, 1318–1327.
43 S. Wang, T. Ishihara and Y. Takita, Partial oxidation of dimethyl ether over various supported metal catalysts, *Appl. Catal., A*, 2002, **228**, 167–176.
44 C. Rioche, S. Kulkarni, F. C. Meunier, J.P. Breen and R. Burch, Steam reforming of model compounds and fast pyrolysis bio-oil on supported noble metal catalysts, *Appl. Catal., B*, 2005, **61**, 130–139.
45 R. Horn, K. A. Williams, N. J. Degenstein and L. D. Schmidt, Syngas by catalytic partial oxidation of methane on rhodium: Mechanistic conclusions from spatially resolved measurements and numerical simulations, *J. Catal.*, 2006, **242**, 92–102.
46 M. Mittal and B. K. Guha, Minimum Ignition Temperature of Polyethylene Dust; a Theoretical Model, *Fire Mater.*, 1997, **21**, 169–177.